Polymer 49 (2008) 3076–3083

Contents lists available at ScienceDirect

Polymer

journal homepage: www.elsevier.com/locate/polymer

Crystallization under shear in isotactic polypropylene containing nucleators

Dmytro Byelov [a,b,c,*], Pierre Panine [d], Klaas Remerie [e], Edwin Biemond [e], Giovanni C. Alfonso [f], Wim H. de Jeu [a,b,c,**]

[a] Dutch Polymer Institute, P.O. Box 902, 5600 AX Eindhoven, The Netherlands
[b] Department of Chemical Engineering and Chemistry, Eindhoven University of Technology, 5600 MB Eindhoven, The Netherlands
[c] FOM Institute for Atomic and Molecular Physics (AMOLF), Kruislaan 407, 1098 SJ Amsterdam, The Netherlands
[d] ESRF, 6 rue Jules Horowitz, 38043 Grenoble, France
[e] SABIC Europe, P.O. Box 319, 6160 AH Geleen, The Netherlands
[f] Department of Chemistry and Industrial Chemistry, University of Genova, Via Dodecaneso 31, 16146 Genova, Italy

ARTICLE INFO

Article history:
Received 12 February 2008
Received in revised form 23 April 2008
Accepted 23 April 2008
Available online 2 May 2008

Keywords:
Polypropylene crystallization
Nucleating agents
Shear

ABSTRACT

We report results from time-resolved small/wide angle X-ray scattering of well-characterized isotactic polypropylene (iPP), in its pure form as well as loaded with nucleating additives of different shapes (isotropic, elongated, platelet-like). Isothermal crystallization of these systems has been studied both under quiescent conditions and after application of a shear pulse. A quantitative analysis is presented that couples the applied shear field and the specific additive to the nucleation of iPP and the subsequent kinetics of crystallization. The effect of flow is only relevant if its contribution to the nucleation density is at least of the same order of magnitude as the nucleation density under quiescent conditions. Anisotropic additives show strong interactions with the flow field leading to extra nucleating sites.

© 2008 Elsevier Ltd. All rights reserved.

1. Introduction

It is well known that the speed of polymer crystallization can be enhanced by the application of flow as well as by mixing in specific additives (nucleating agents). Under strong shear conditions, nucleation changes from isotropic (followed by the growth of spherulites) to anisotropic (row nucleation, followed by the growth of shish–kebab structures or by the development of a transcrystalline morphology) [1–5]. Similar effects can be induced by heterogeneities in the melt (i.e. additives) that are often used during polymer processing. The presence of various additives in commodity polymers like isotactic polypropylene (iPP) is quite common but is seldom properly specified. Consequently, results from various publications on the crystallization of iPP from different commercial sources cannot be easily compared. Accordingly, the underlying mechanisms are still poorly understood in spite of the large amount of work over the last decades. In this paper we report results from small/wide angle X-ray scattering (SAXS/WAXS) studies of the crystallization of a well-characterized iPP loaded with selected nucleating agents, both under quiescent conditions and after a mild shear pulse. The thermo-mechanical history of the experiments has been carefully considered and the data are referred to the same crystallization temperature. The objective is to quantify the role that the applied shear field, which may be coupled to a specific additive, has on the formation of precursor structures (nuclei) in the polymer melt. The latter will, in turn, influence the kinetics of crystallization. The protocol chosen is such that crystallization only starts after the end of the shear pulse. Hence we do not enter the regime of row nucleation and no shear is exerted on the crystals (in contrast to, for example, the situation in Ref. [6]). It turns out that elongated and platelet-like additives do interact with the flow field producing extra nucleating sites. The isotropic nucleant is so effective that it masks any possible effect of shear.

2. Experimental

IPP with characteristics $M_w = 790$ kg/mol and $M_n = 155$ kg/mol was obtained from Sabic Europe. This starting material was of high purity and contained as only additive 0.2% of the stabilizer (antioxidant) Irganox B225. The melting point was 164 °C. The stabiliser and small concentrations (0.05%, 0.1% and 0.2%) of the selected nucleating agent were mixed with the pure iPP powder at SABIC using a Henschell mixer. This mixture was placed in the hopper of a ZSK30 co-rotating twin-screw extruder (length/diameter ratio of

* Corresponding author. Present address: Van't Hoff Laboratory for Physical and Colloid Chemistry, Debye Institute, Utrecht University, Padualaan 8, 3584 CH Utrecht, The Netherlands. Tel.: +31 302532540.
** Corresponding author. Present address: Polymer Science and Engineering, University of Massachusetts, 120 Governors Drive, Amherst, MA 01003, USA.
E-mail addresses: d.byelov@uu.nl (D. Byelov), dejeu@mail.pse.umass.edu (W.H. de Jeu).

0032-3861/$ – see front matter © 2008 Elsevier Ltd. All rights reserved.
doi:10.1016/j.polymer.2008.04.051

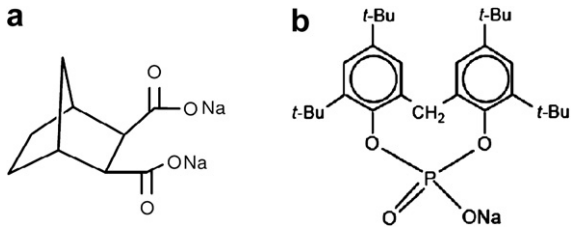

Fig. 1. Structural formulas of two of the nucleation agents used: (a) HPN68L – *cis-endo*-bicyclo[2.2.1]heptane 2,3-carboxylate disodium salt; (b) NA11UH – 2,2′-methylene bis(4,6-di-*tert*-butylphenol) phosphate sodium salt.

33 at a throughput of 10 kg/h and a barrel temperature of 240 °C). Special care was taken to avoid even the slightest contamination with additives used in other compounds.

Three types of additives were used. Two of them are especially designed as nucleants for iPP and commercialized under the names HPN68L (Milliken, USA) and NA11UH (Adeka, Japan), respectively. The main ingredient of HPN68L is *cis-endo*-bicyclo[2.2.1]heptane 2,3-carboxylate disodium salt (Fig. 1a), which has approximately an isotropic morphology. It also contains several other components to prevent particle agglomeration under the influence of moisture outside the polymer. The initial particles' size is defined as $D_{95} < 10$ μm – 95% of the particles are smaller than 10 μm (Fig. 2a). Upon mixing into the polymer, the particles of the additive break up into smaller pieces, less than 1 μm in case of a good dispersion [7a]. The second nucleating agent, NA11UH, is the latest ultra-fine version of NA11 and consists of: 2,2′-methylene bis(4,6-di-*tert*-butylphenol) phosphate sodium salt (Fig. 1b). NA11UH is insoluble in the PP melt under processing conditions, and therefore dispersed as a finely divided solid. The particle sizes of this additive are distributed according to $D_{90} < 14$ μm, $D_{50} < 4$ μm and $D_{10} < 1$ μm [7a]. The particles have an elongated morphology [8] and from Fig. 2b we can conclude they have a broad range of aspect ratios. As third type of additive talcum powder was used which has a platelet-like morphology (Fig. 2c). The melting point of all additives is much higher than the annealing temperature used in our experimental protocol.

Isothermal crystallization experiments (both quiescent and after shear) were carried out in a modified Linkam CSS450 temperature-controlled shear system (parallel plate geometry). To allow X-ray scattering experiments the original glass windows were replaced by kapton foils with a thickness of 130 μm. The system was loaded with about 1 mm thick discs of iPP, pressed beforehand in a homemade setup for 10 min at about 3 kPa in a vacuum oven at 220 °C. The following measurement protocol was used:

- For each measurement a new iPP disc was annealed in the shear system for 1 min at 195 °C, squeezed to a thickness 0.8 mm and further annealed for another 4 min.
- After annealing, the sample was squeezed to the final thickness of 0.6 mm and cooled down at 30 °C/min to the crystallization temperature of 136 °C, 28 °C below the melting point.
- Upon reaching the crystallization temperature, a steady shear pulse was applied with a rate $\dot{\gamma} = 10\ s^{-1}$ during 1 s at the fixed gap of 0.6 mm.

We noted that the modified shear cell has considerable temperature gradients. However, as a strict protocol was applied this should not affect the comparison of the various crystallization situations, but the absolute numbers given are less precise. Scattering experiments were performed at beamline ID2 of the European Synchrotron Radiation Facility (ESRF, Grenoble) at a wavelength $\lambda = 0.0995$ nm. The combined SAXS/WAXS setup has been described in detail elsewhere [9]. The distance from sample to SAXS-detector was set to 3 m providing a q-range from 0.3 nm^{-1} to 1.6 nm^{-1}. For WAXS a q-range from 4 nm^{-1} to 40 nm^{-1} was covered. Additional measurements were done using an in-house setup described earlier [10]. The two-dimensional SAXS intensity was first integrated azimuthally (Fig. 3a) to obtain the scattering pattern as a function of $q = (4\pi/\lambda)\sin\theta$, the modulus of the momentum transfer vector $\mathbf{q}$, 2θ being the scattering angle (see Fig. 3b). In SAXS the scattering arises from the 'the two-phase system' of crystalline/amorphous domains. In this situation the product of the volume fractions of the two phases is proportional to the so-called invariant $\int I(q)q^2 dq$ [11]. Taking the limited experimental q-range into account we then follow the development of crystallization by estimating the relative, time-dependent invariant from the expression:

$$Q_r(t) = \int_{q_{min}}^{q_{max}} I(q,t)q^2 dq. \quad (1)$$

In addition to the SAXS also WAXS data were incorporated that provide information on the crystallographic registry. Hence the WAXS intensity is directly proportional to the concentration of the crystalline phase. Thus after decomposition into contributions from the amorphous and from the crystalline parts of the sample, the absolute crystallinity can be obtained. The amorphous halo has been measured immediately after quenching; in this situation no indication of a crystal peak is detected in the scattering curve. Subsequently the final scattering is background subtracted and compared to the scaled amorphous pattern. Scaling has been performed in two ways. In the first method the maximum of the amorphous halo is normalized to the minimum between the $(110)_\alpha$ and the $(040)_\alpha$ crystalline diffraction peaks. In the second case the intensity at the wings of the amorphous halo (low and high-q regions) is normalized to the intensity at the wings of the full crystalline-plus-amorphous scattering pattern. The first method can be expected to overestimate the amount of amorphous material

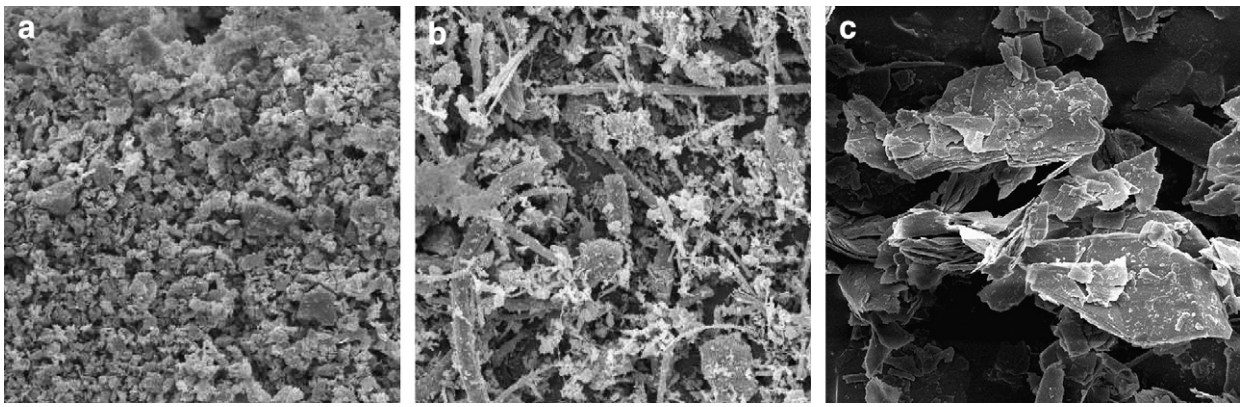

Fig. 2. Scanning electron microscopic images (40×40 μm^2) of various nucleants. (a) Isotropic HPN68L. (b) Elongated NA11UH. (c) Platelet-like talcum.

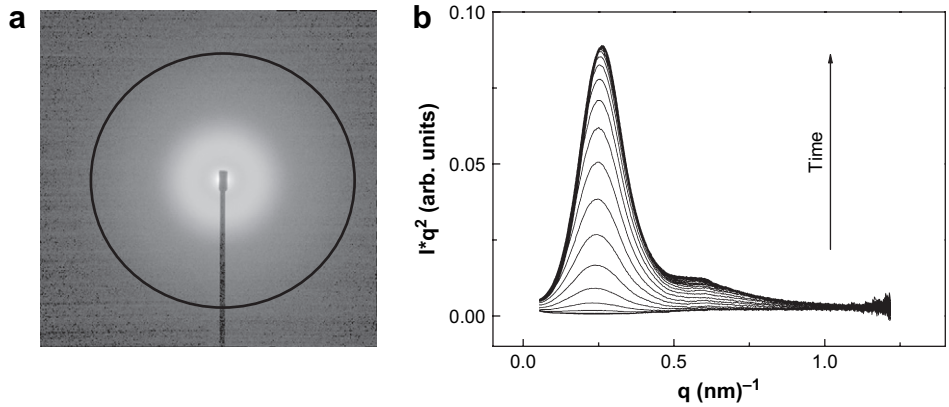

Fig. 3. SAXS of crystallization of pure iPP. (a) Two-dimensional intensity distribution. (b) Azimuthally integrated intensity indicating the development of a lamellar crystalline morphology. Note the second-order peak as a 'bump' at larger q-values.

somewhat; however, the difference between both methods lies in the range of 2% only. For a critical evaluation of the procedure we refer to Ref. [12]. Once the scaled amorphous pattern is subtracted from the total signal (see Fig. 4) the absolute crystallinity can be calculated from

$$X_{\mathrm{abs}} = \frac{X_{\mathrm{c}}}{X_{\mathrm{c}} + X_{\mathrm{a}}}. \tag{2}$$

In this formula X_{c} is the intensity of crystalline peaks integrated between two limits:

$$X_{\mathrm{c}} = \int_{q_1}^{q_2} I_{\mathrm{c}}(q)\mathrm{d}q, \tag{3}$$

and $X_{\mathrm{c}} + X_{\mathrm{a}}$ represents the total scattered intensity (without amorphous halo subtraction) integrated between the same limits:

$$X_{\mathrm{c}} + X_{\mathrm{a}} = \int_{q_1}^{q_2} I_{\mathrm{c+a}}(q)\mathrm{d}q. \tag{4}$$

For all our samples the fraction of the crystalline phase at the end of the process is $44 \pm 5\%$. It is worth to mention that for the future analysis we need to know only the relative crystallinity $X_{\mathrm{rel}}(t) = Q_{\mathrm{r}}(t)/Q_{\mathrm{r}}(\infty)$.

The halftime of crystallization $\tau_{1/2}$ can be calculated in various ways. We have systematically taken the maximum of the derivative of the crystallization curve. This was accomplished by approximating the crystallization curve by a B-spline of the third order and subsequently calculating its derivative [13]. This way of determining $\tau_{1/2}$ has the advantage that the result does not depend on the quality or completeness of the measurement of the saturated part of the crystallization curve, or on its normalization. In fact $\tau_{1/2}$ defined in this way does not exactly corresponds to 50% crystallinity but to 48.7%. For simplicity the notation $\tau_{1/2}$ will still be used. In Fig. 5 the crystallization kinetics in quiescent conditions from SAXS and WAXS experiments is compared. In this figure we scaled the absolute crystallinity from the WAXS to a relative scale in order to make comparison clearer. Since the results are in close agreement (the range of errors is less then 5%), further discussion will be based on the SAXS data. It is important to mention that iPP is a polymorphic material and crystal morphology can be modified by specific nucleants or experimental conditions. For our samples, both pure and in presence of additives WAXS experiments showed that only the α crystal phase was present.

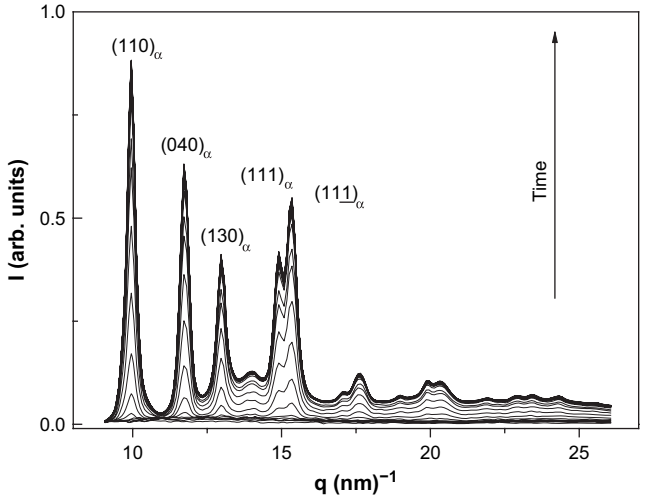

Fig. 4. Time-resolved WAXS reflecting the development of crystalline order in pure iPP.

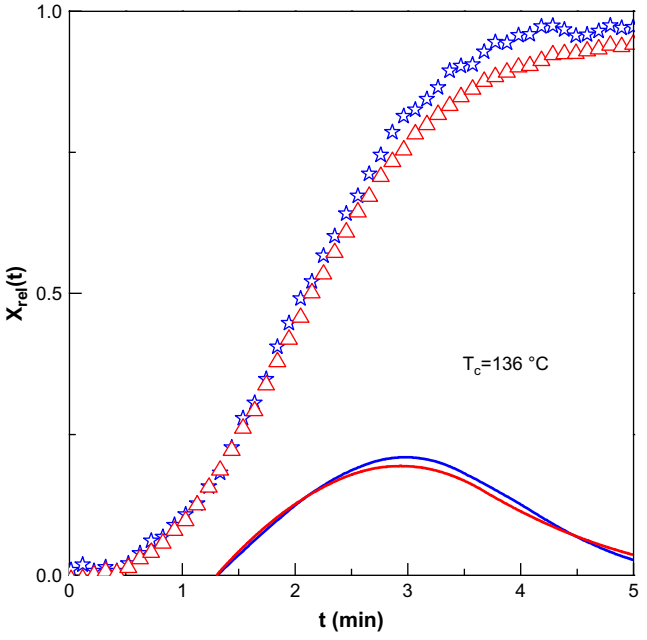

Fig. 5. Relative crystallinity in iPP-I1 from SAXS (blue stars) and from WAXS (red triangles), respectively. To highlight the inflexion point the derivatives of the $X_{\mathrm{rel}}(t)$ curves are given as continuous blue and red lines (arbitrary vertical scale; horizontally shifted over 1 min for clarity). (For interpretation of the references to colour in this figure legend, the reader is referred to the web version of this article.)

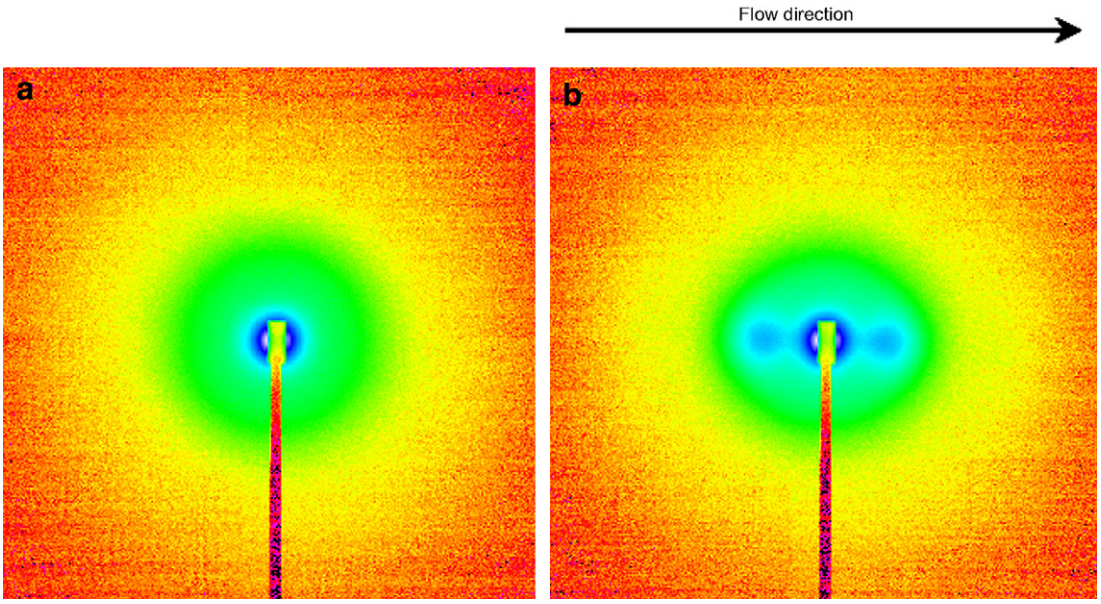

Fig. 6. Crystallization of pure iPP at 136 °C. (a) Quiescent. (b) After shearing with 10 s^{-1} for 1 s.

3. Results

3.1. Pure iPP

Fig. 6a shows a 2D synchrotron SAXS image of pure iPP during the crystallization process. The broad isotropic peak at $q = 0.25$ nm^{-1} corresponds to the formation of the lamellar crystalline structure. Under quiescent conditions we did not observe any anisotropy in the scattering pattern. Application of shear causes orientation of the peak in the flow direction (equatorial, see Fig. 6b). This indicates orientational order in the melt of pure iPP, which in turn leads to the formation of an oriented crystalline lamellar stacking in the crystallized material. However, we did not observe a meridional streak at the early stage of crystallization. Indeed, the shish–kebab scenario does not apply to the present range of mild shear values used.

The development with time of the crystalline structure in pure iPP is shown in Fig. 7 together with the derivative of crystallization curves. The resulting values for $\tau_{1/2}$ are summarized in Table 1. The halftime of crystallization for sheared iPP is approximately three times smaller than that under quiescent conditions.

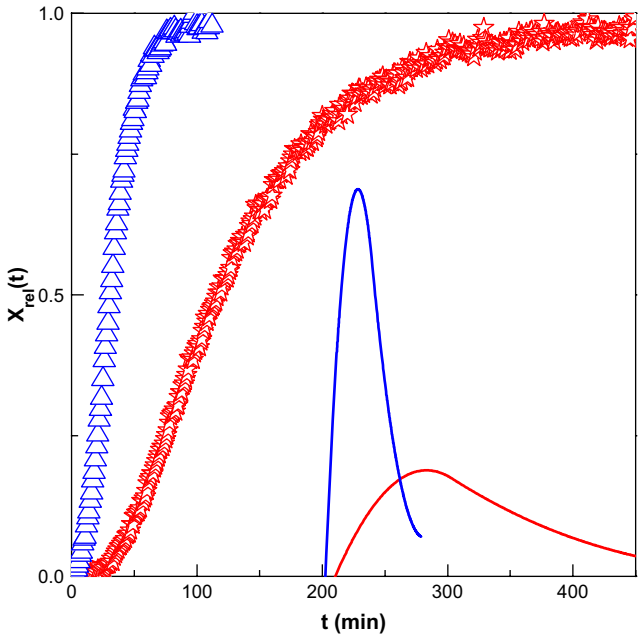

Fig. 7. Relative crystallinity in iPP from SAXS. Red stars – quiescent crystallization; blue triangles – crystallization after shear. The continuous red and blue lines represent the derivative of the corresponding $X_{rel}(t)$ curves (arbitrary vertical scale; horizontally shifted over 200 min for clarity). (For interpretation of the references to colour in this figure legend, the reader is referred to the web version of this article.)

3.2. iPP loaded with the isotropic nucleating agent (iPP-I)

Qualitatively the scattering patterns from iPP nucleated with the isotropic agent HPN68L do not differ from those of pure iPP. The position of the broad isotropic peak is the same as for the pure iPP. However, the kinetics of crystallization changes dramatically (see Fig. 8). For iPP loaded with 0.05% of HPN68L $\tau_{1/2}$ is about 50 times shorter than for pure iPP (see Table 1). At higher content of the nucleant, $\tau_{1/2}$ decreases by another factor of two. Most importantly, for this system additional shear has only a minor effect on the kinetics of crystallization. Evidently, any effect of shear on iPP itself is overwhelmed by the strong nucleation due to the additive that is hardly influenced by the shear under the present experimental conditions.

Table 1
Composition of the samples and halftime of crystallization as measured using the experimental protocol described in the text

Sample	Nucleant	Content (wt%)	Quiescent $\tau_{1/2}$ (s)	Sheared $\tau_{1/2}$ (s)
IPP	–	–	5000	1700
IPP-I1	HPN68L (isotropic)	0.05	120	120
IPP-I2		0.1	70	75
IPP-I3		0.2	60	65
IPP-E1	NA11UH (elongated)	0.05	3800	700
IPP-E2		0.1	1500	600
IPP-E3		0.2	230	180
IPP-P1	Talcum (platelets)	0.1	900	350
IPP-P2		0.2	610	270
IPP-P3		0.5	700	210

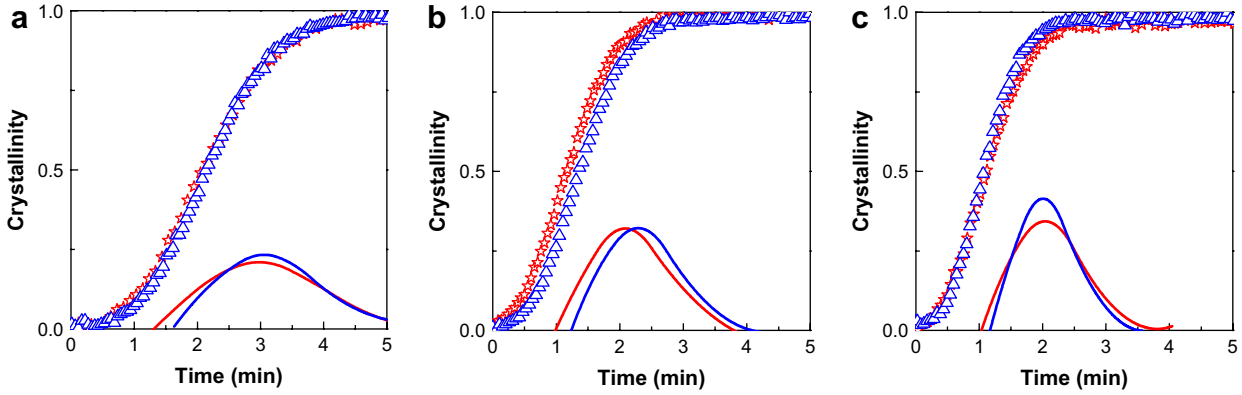

Fig. 8. Relative crystallinity of iPP samples loaded with the isotropic nucleant HPN68L at concentrations of 0.05% (a), 0.1% (b) and 0.2% (c), respectively. Red stars – quiescent crystallization; blue triangles – crystallization after shear. The continuous red and blue lines represent the derivative of the corresponding $X_{rel}(t)$ curves (arbitrary vertical scale; horizontally shifted over 1 min for clarity). (For interpretation of the references to colour in this figure legend, the reader is referred to the web version of this article.)

3.3. iPP loaded with the elongated nucleating agent (iPP-E)

The effect of loading iPP with the elongated nucleator NA11UH is rather unexpected. Already at quiescent crystallization some orientation already appears in the scattering pattern (see Fig. 9a). This effect is reproducible within the framework of our experimental protocol. Application of external shear changes the direction of orientation to along the applied shear flow (Fig. 9b). Similar observations have been recently reported for the different system of poly(butylene terephthalate) loaded with single wall carbon nanotubes [14]. The effect of NA11UH on the kinetics of crystallization is weaker than observed for HPN68L, especially at low concentrations (Fig. 10a). However, application of shear now has an appreciable effect on decreasing the halftime of crystallization. For 0.05 wt% and 0.1 wt% of NA11UH the effect of shear is comparable to that in pure iPP. For a concentration 0.2 wt% of NA11UH the effect of shear is minor (see Table 1).

3.4. iPP loaded with the platelet-like nucleating agent (iPP-P)

Qualitatively the 2D scattering patterns from iPP loaded with talcum do not differ from those of pure iPP and iPP nucleated with isotropic agent HPN68L. The kinetics of crystallization for the samples nucleated with talcum is comparable to the ones nucleated with NA11UH (see Table 1). Application of shear further decreases the halftime of crystallization as expected. For equivalent concentrations of nucleants the effect is even more pronounced than for iPP nucleated with NA11UH (Fig. 10b).

4. Discussion

One key issue to understand our experimental results is nucleation. Hence we should consider the relative fraction of nuclei generated by the different mechanisms. The focus here is not to provide an accurate quantitative description of the density of nucleating centres, rather to reveal the main phenomenological aspects of coupling of nucleating agents and applied shear fields.

For isobaric experiments of isothermal crystallization at T_c the following contributions to nucleation density (number of nucleation sites per unit volume) should be considered.

- $N_{hom}(T_c, t)$ – Homogeneous nuclei generated in the system by thermally activated local density fluctuations whenever the material is supercooled. Their concentration increases linearly in time with a temperature dependent rate $\dot{N}(T)$.
- $N^0_{het}(T_c)$ – This contribution includes all nuclei that are due to contamination of the material (catalyst residues, dust, etc.) and to possible remnants of order left in the system if the melt is not fully annealed. It also includes any possible nucleation effect of the kapton windows of the sample cell. This is an important intrinsic and unavoidable contribution to

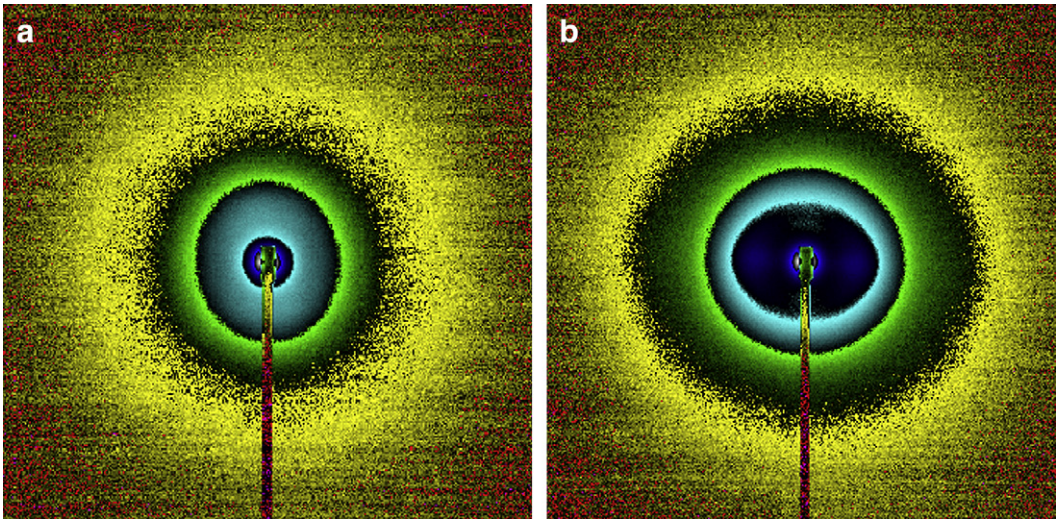

Fig. 9. Crystallization of iPP loaded with the elongated nucleant NA11UH. (a) Quiescent. (b) After shearing with 10 s^{-1} for 1 s.

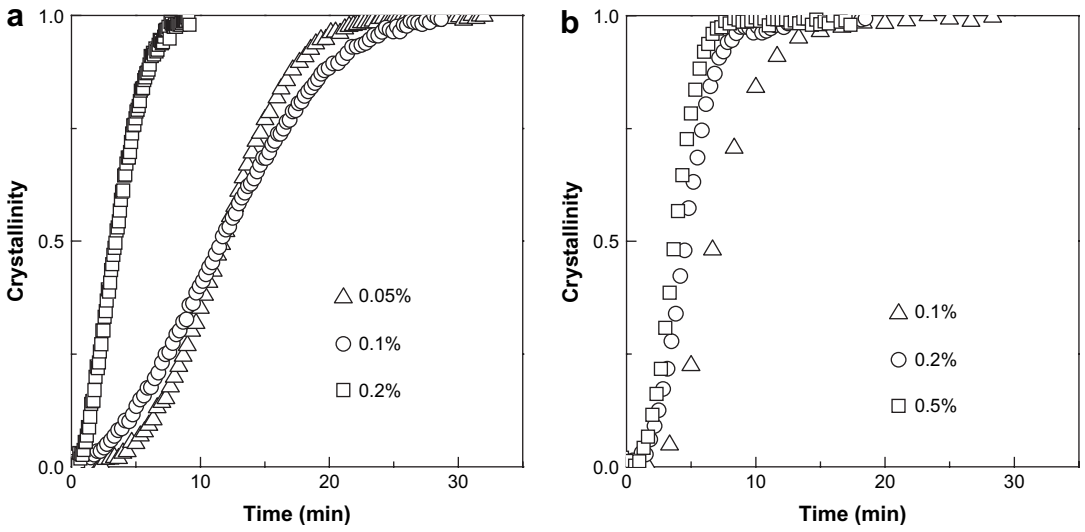

Fig. 10. Relative crystallinity of sheared iPP samples. (a) Loaded with the elongated nucleant NA11UH at the concentrations indicated; (b) ibid with talcum.

crystallization in all polymers of industrial origin. There are very few polymers for which $N^0_{het}(T_c)$ is small, for example PHB extracted from bacteria.

- $N^A_{het}(T_c)$ – This contribution originates from added nucleating substances. Its relevance obviously depends on the nature of the additive, its concentration and specific surface area per unit mass, features of the surface, etc.

In our reference experiments on quiescent crystallization, the number of nuclei corresponds to $N_{ref} \equiv N_{hom}(T_c, t) + N^0_{het}(T_c)$. The intrinsic nature of the second contribution makes it difficult to separate the two effects. The only way to do so is to exploit the time dependence of N_{hom}. However, in many practical situations N_{hom} is small and can be disregarded, especially for short crystallization times.

In the case of crystallization after application of shear (at a shear rate $\dot{\gamma}$ and temperature T_s during a time window t_s) an additional contribution $N_s(T_c, T_s, t_s, \dot{\gamma}, M)$ must be taken into account. We assume this contribution is due to the direct effect of shear on the polymer itself; any possible effect of the shear on N^0_{het} is assumed to be small compared to N_s. Another possible source of nuclei could arise from the interactions between the flow field and the added nucleating particles. The latter contribution can be expected to depend on N^A_{het} and will be denoted by ΔN^A_s. Confrontation of this division in various contributions to the nucleation density with the experimental data should show which factors are most important and whether this model is sufficiently complete.

Focussing the discussion on N_s, we note that for a mild step shear, imposed when the sample reaches T_c (hence $T_s = T_c$), the number of nuclei per unit volume increases linearly with the shearing time [2,15]:

$$N_s = \beta t_s. \tag{5}$$

Here β is the rate of injection of flow-induced nuclei in the system. Its dependence on material characteristics and shear conditions is well described by the empirical equation [15]:

$$\beta = \beta_0 \dot{\gamma}^2 \exp\left(\frac{A}{RT_s}\right), \tag{6}$$

in which $\beta_0 = \beta_0(M_w)$ is still a function of the average molecular weight and the constant A accounts for the temperature dependence of shear-induced nucleation.

Experimentally the number of nucleation sites N can be extracted from the progress of crystallinity assuming that the Kolmogoroff–Avrami–Evans equation [16,17] holds:

$$X(t) = 1 - \exp\left(-\frac{4\pi}{3} N G^3 t^3\right), \tag{7}$$

in which N represents the number of nuclei in the sample and G the growth rate of spherulites. The coefficient $4\pi/3$ relates to the assumed spherical geometry of the crystallites. This assumption should hold for our experimental conditions of crystal growth only occurring after cessation of a mild shear pulse. This is confirmed by optical microscopic measurements demonstrating that we are in the regime of point-like nucleation. The exponent of t is taken equal to 3 as we are concerned with 3D isotropic growth on predetermined nuclei. The results are shown in Fig. 11, and indicate that the cubic power holds well for the initial part of the crystallization with which we are mainly concerned. The number of nuclei can be estimated by rewriting Eq. (7) in the form:

$$N = -\frac{3}{4\pi G^3} \frac{\ln(1-X)}{t^3} \equiv \frac{B}{t^3}. \tag{8}$$

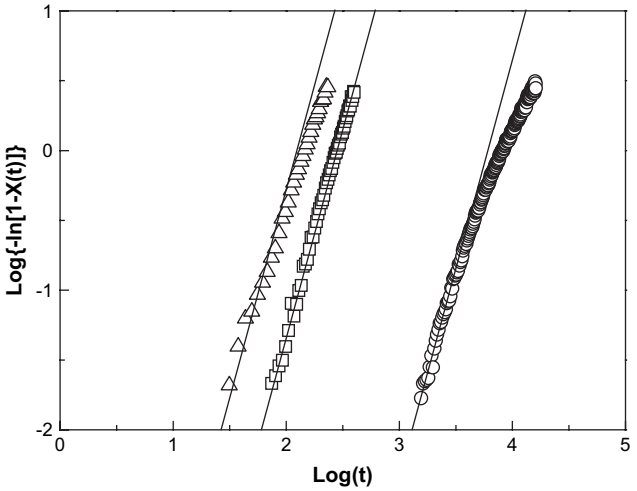

Fig. 11. Illustration of 3D isotropic growth on predetermined nuclei. Black circles – pure iPP; red triangles – iPP nucleated with HPN68L; red boxes – iPP nucleated with NA11UH; solid line – fit to Eq. (7).

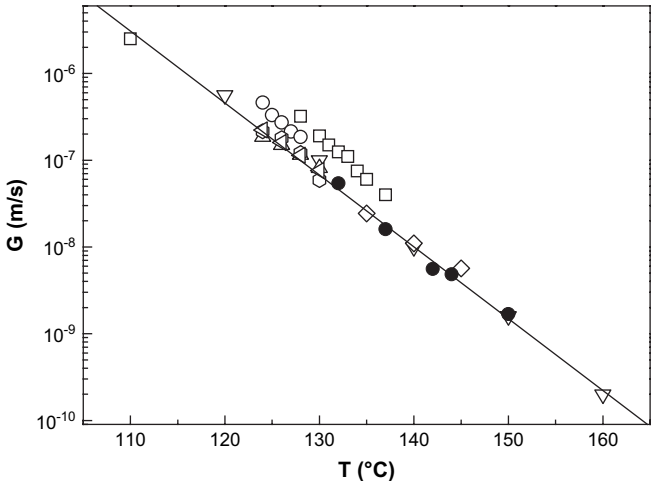

Fig. 12. Temperature dependence of the growth rate of spherulites of iPP. Open symbols – collection of industrial Ziegler–Natta iPP from the literature; filled circles – data for the present pure iPP from Sabic.

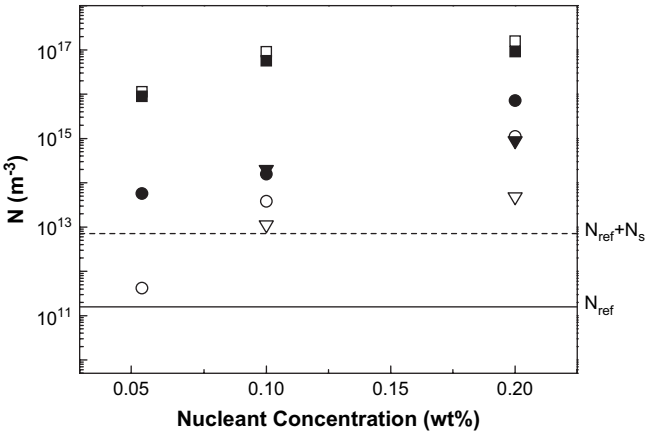

Fig. 13. Number of nucleating sites in iPP as obtained from the experiments. Solid line – pure iPP at quiescent conditions; dashed line – pure iPP sheared; squares – iPP nucleated with HPN68L; circles – iPP nucleated with NA11UH; triangles – iPP nucleated with talcum. Open symbols correspond to quiescent conditions, filled symbols to crystallization after shear.

As we see, information on G is needed to calculate the nucleation density from our crystallization data. Note that the analysis as presented only requires knowledge of the relative crystallinity.

Fig. 12 shows a collection of literature data on the growth rate of typical industrial Ziegler–Natta iPP [18–22]. G appears to be rather independent of M_w and does not vary much between iPP from different sources. Systematic measurements on our pure iPP sample from SABIC (Fig. 12, filled symbols) are in a good agreement with the literature data. From these results we estimate that the linear growth rate of iPP at 136 °C to be 1.304 μm/min = 2.17×10^{-8} m/s. This value corresponds to the deposition of about twenty stems per second on the growing crystal face.

To discuss the nucleation densities quantitatively we shall base our discussion on $\tau_{1/10}$, the time needed to get a relative crystallinity $X = 0.1$. By selecting this value we expect less interference between growing crystallites than for $X = 0.5$ and also a reduced contribution from $N_{hom}(T_c,t)$. Introducing these choices in Eq. (8) the overall nucleation density can be written as

$$N = \frac{B}{\left(\tau_{1/10}\right)^3} \tag{9}$$

in which $B = 2.71 \times 10^{24}$ s^3 m^{-3}. On the basis of this equation we have evaluated the nucleation density for the various experimental situations, see Table 2. The results are summarized in graphical form in Fig. 13. The nucleation density of sheared pure iPP is 7.1×10^{12} nuclei/m^3, which is considerably larger than the nucleation density of the pure polymer under quiescent conditions (1.6×10^{11} nuclei/m^3).

Table 2
Experimentally determined number of nuclei per cubic meter at $X_{rel} = 0.1$

Sample	$N_{hom} + N^0_{het} \equiv N_{ref}$	$N_{ref} + N_s$	$N_{ref} + N^A_{het}$	N^A_{het}	$N_{ref} + N^A_{het} + N_s + \Delta N^A_s$
iPP	1.6×10^{11}	7.1×10^{12}	–	–	7.1×10^{12}
IPP-I1	–	–	1.1×10^{16}	1.1×10^{16}	8.9×10^{15}
IPP-I2	–	–	9.1×10^{16}	9.1×10^{16}	5.7×10^{16}
IPP-I3	–	–	1.6×10^{17}	1.6×10^{17}	9.1×10^{16}
IPP-E1	–	–	4.2×10^{11}	2.6×10^{11}	5.7×10^{13}
IPP-E2	–	–	3.8×10^{13}	3.8×10^{13}	1.6×10^{14}
IPP-E3	–	–	1.1×10^{15}	1.1×10^{15}	7.1×10^{15}
IPP-P1	–	–	1.1×10^{13}	1.1×10^{13}	2.0×10^{14}
IPP-P2	–	–	4.8×10^{13}	4.8×10^{13}	8.9×10^{14}
IPP-P3	–	–	3.8×10^{13}	3.8×10^{13}	1.6×10^{15}

Nucleant HPN68L is extremely efficient and provides already at 0.1 wt% a nucleation density around 10^{17} nuclei/m^3, six orders of magnitude larger than for pure iPP under quiescent conditions. The concentration of heterogeneous nuclei is so large that any additional effect of flow, as expressed in N_s (and possibly ΔN^A_s) becomes irrelevant. Whether prolonged shear could produce a number of nuclei sufficient to decrease the crystallization halftime any further, still remains an open question. On the basis of Eq. (6) we estimate that such an effect could be possible at a shear rate around 1000 s^{-1} applied for 1 s or alternatively a rate of 30 s^{-1} for 1000 s.

The nucleant NA11UH gives under quiescent conditions and for concentrations of 0.05 wt% and 0.1 wt% the same order of magnitude of nuclei as sheared pure iPP. However, 0.2 wt% leads to two orders of magnitude more nuclei. The 'nucleating power' of both nucleants is compared in Table 2. Interestingly for NA11UH already without any shear the crystallization is strongly anisotropic. We have been tempted to attribute this to pressure-induced orientation during sample preparation. However, in that case one would not expect the observed rather uniform orientation in the plane of the discs. For the moment this question remains open. Upon applying shear the orientation of the crystallization becomes parallel to the velocity direction, similar to all other cases.

Under quiescent conditions, talcum (the final nucleant) gives the same order of magnitude of nuclei as the sheared pure iPP. A small increase in the number of nuclei is observed between 0.1 wt% and 0.2 wt% and hardly further changes occur for 0.5 wt% (Table 2). The effect of shear for the samples with talcum is comparable to the effect of shear on pure iPP (see Fig. 13).

So far we have implicitly assumed that the various contributions to the nucleation density are simply additive. Only when the contributions to the nucleation density from the various mechanisms are of the same order of magnitude, this point can be checked. This is the case for iPP nucleated with NA11UH at concentrations of 0.05 wt% (iPP-E1) and 0.1 wt% (iPP-E2) and for iPP nucleated with talcum. In the first case we find for the overall nucleation density (see Table 2) $N_{sum} = N_{hom} + N^0_{het} + N^A_{het} + N_s = 7.4 \times 10^{12}$ nuclei/m^3 while experimentally the last row gives for iPP-E1 $N_{exp} = 5.7 \times 10^{13}$ nuclei/m^3. For iPP-E2 these numbers are $N_{sum} = 4.5 \times 10^{13}$ nuclei/m^3 and $N_{exp} = 1.6 \times 10^{14}$ nuclei/m^3. In both cases N_{exp} is appreciably higher than N_{sum} indicating a non-zero value ΔN^A_{het} of the order of 10^{13} nuclei/m^3. This shows that the elongated particles of NA11UH interact with the flow field to produce further nuclei. Similar considerations apply to the anisotropic talcum particles in the samples iPP-P1, iPP-P2 and iPP-P3. We find

in these cases $N_{sum} = 1.8 \times 10^{13}$ nuclei/m^3, $N_{sum} = 5.5 \times 10^{13}$ nuclei/m^3, $N_{sum} = 4.5 \times 10^{13}$ nuclei/m^3, respectively, while N_{exp} is of the order of 10^{15} nuclei/m^3. In the case of carbon nanotubes as additive [14] it has been suggested that for sheared samples the anisotropic particles counterbalance nuclei relaxation by providing surfaces which stabilize some of them. A similar mechanism could apply to our anisotropic additives in iPP. Unfortunately, at this stage these observations cannot be compared with an isotropic nucleant of similar effectiveness.

5. Conclusions

The crystallization of iPP has been studied under quiescent conditions as well as under mild shear, on pure iPP as well as with iPP containing nucleating agents. Good agreement has been obtained for the halftime of crystallization $\tau_{1/2}$ as determined by SAXS and by WAXS. For pure iPP we reproduce the well-known decrease in $\tau_{1/2}$ upon shearing. Addition of the isotropic nucleation agent HPN68L leads to a strong increase of the speed of quiescent crystallization (number density of nucleating sites). This large increase masks any possible effect of shear. The effect of flow only manifests itself if its contribution to the nucleation density is of the same order of magnitude as that under quiescent conditions. This situation applies to the elongated nucleating agent NA11UH and to the platelet-like talcum, which are both less effective than the isotropic nucleator HPN68L. This allows decomposing the contributions to the nucleation density in iPP from the shear field and from the nucleating agent in a semi-quantitative way. The results suggest that the elongated and platelet-like particles of the additive strongly interact with the flow field producing extra nucleating sites. Elucidation of the possible mechanisms involved still constitutes a considerable challenge.

Acknowledgement

We thank Anne Spoelstra (Eindhoven) for carrying out the SEM measurements. This work is part of the Research Programme of the Dutch Polymer Institute (DPI), project #553.

References

[1] Keller A, Kolnaar HWH. In: Meijer HEH, editor. Processing of polymers, vol. 18. VCH; 1997. p. 189.
[2] Eder G, Janeschitz-Kriegl H. In: Meijer HEH, editor. Processing of polymers, vol. 18. VCH; 1997. p. 269.
[3] Kornfield JA, Kumaraswamy G, Issaian AM. Ind Eng Chem Res 2002;41:6383.
[4] Somani RH, Yang L, Zhu L, Hsiao BS. Polymer 2005;46:8587.
[5] Van Meerveld J, Peters GWM, Hütter M. Rheol Acta 2004;44:119.
[6] Haudin J-M, Duplay C, Monasse B, Costa JC. Macromol Symp 2002;185:119.
[7] (a) Hanssen R. (Milliken Europe), private communication.
(b) Green R. (Adeka-Palmarole), private communication.
[8] Nagasawa S, Fujimori A, Masuko T, Iguchi M. Polymer 2005;46:5241.
[9] Panine P, Urban V, Boesecke P, Narayanan T. J Appl Crystallogr 2003;36:991.
[10] Li L, de Jeu WH. Macromolecules 2004;37:5646.
[11] Porod G. In: Kratky OGO, editor. Small angle X-ray scattering. Academic Press; 1982.
[12] Van der Burgt FPTJ, Rastogi S, Chadwick JC, Rieger B. J Macromol Sci B Phys 2002;41:1091.
[13] de Boor C. A practical guide to splines. Springer-Verlag; 1978.
[14] García-Gutiérrez MC, Hernández JJ, Nogales A, Panine P, Rueda DR, Ezquerra TA. Macromolecules 2008;41:844.
[15] Alfonso GC, Azzurri F. Formation and disappearance of shear induced nucleation precursors. In: Proceedings of the meeting polymer crystallization and structure formation in processing. Linz, Austria; November 2003.
[16] Kolmogoroff AN. Izv Akad Nauk SSSR Ser Math 1937;3:355.
[17] Avrami M. J Chem Phys 1939;7:1103.
[18] Li J, Shanks RA, Long Y. Polymer 2001;42:1941.
[19] Jang GS, Cho WJ, Ha CS. J Polym Sci Part B Polym Phys 2001;39:1001.
[20] Wang K, Wu J, Zeng H. Eur Polym J 2003;39:1647.
[21] Janeschitz-Kriegl H. Macromolecules 2006;39:4448.
[22] Chen JH, Yao BX, Su WB, Yang YB. Polymer 2007;48:1756.